THE JOURNAL OF PHYSICAL CHEMISTRY LETTERS
A JOURNAL OF THE AMERICAN CHEMICAL SOCIETY

pubs.acs.org/JPCL

Letter

# Facile Removal of Bulk Oxygen Vacancy Defects in Metal Oxides Driven by Hydrogen-Dopant Evaporation

Min Hu, Qing Zhu, Yuan Zhao, Guozhen Zhang, Chongwen Zou, Oleg Prezhdo, and Jun Jiang*

Cite This: *J. Phys. Chem. Lett.* 2021, 12, 9579–9583

Read Online

ACCESS | Metrics & More | Article Recommendations | Supporting Information

**ABSTRACT:** Oxygen vacancy is a common defect in metal oxides that causes appreciable damage to material properties and performance. Removing bulk defects of oxygen vacancy ($V_O$) typically needs harsh conditions such as high-temperature annealing. Supported by first-principles simulations, we propose an effective strategy of removing $V_O$ bulk defects in metal oxides by evaporating hydrogen dopants. The hydrogen dopants not only lower the migration barrier of $V_O$ but also push $V_O$ away due to their repulsive interaction. The coevaporation mechanism was supported by a neural networks potential-based molecular dynamics simulation, which shows that the migration of hydrogen dopants from inside to surface at 400 K promotes the migration of $V_O$ as well. Our proof-of-concept study suggests an alternative and efficient way of modulating oxygen vacancies in metal oxides via reversible hydrogen doping.

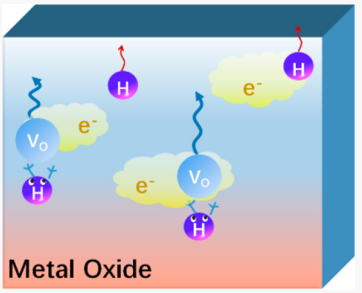




Bulk defects have been regarded as a critical factor that damages properties and performance of solid materials.[1,2] Processing of electronic materials and devices is often jeopardized by defects that capture electrons and block their transport.[3,4] Photoelectric conversion in photovoltaic and photocatalytic semiconductors can be severely suppressed by defects that recombine photogenerated charges.[5−7] Surface defects on catalysts can serve as active sites, while the unwanted bulk defects always hurt the delivery of energetic charges.[8,9] Although oxygen vacancies ($V_O$) in some metal oxide materials favor solar-fuel photocatalyst applications by forming the conductive channel and prolonging the electron lifetime,[10] playing an important role in catalysis,[11] they may occur at various locations in the bulk, where they are extremely difficult to remove or control. In addition, the formation of oxygen vacancies may prevent useful metal-to-insulator phase transitions.[12]

Many strategies have been proposed to remove $V_O$ defects in the bulk, such as thermal annealing and plasma treatment.[13−15] Thermal annealing (Figure 1a) is widely applied to repair vacancy defects. It bestows $V_O$ with kinetic energy, driving $V_O$ to move and resulting in more organized systems with lower energy. However, high operating temperature makes thermal annealing and plasma treatment energy demanding and environmentally unfriendly.[16] These methods also lead to side reactions such as phase transitions. It is thus a pressing issue to develop cost-effective strategies for removing $V_O$ defects in metal oxides under mild conditions.

Hydrogenation could be a potential approach to repair structural defects in metal oxides.[17] Zou et al. found that the oxygen vacancies of $VO_2$ could be repaired quickly as it was treated by hydrogen doping.[18] Because we have developed a cost-effective acid−metal treatment for hydrogen doping of

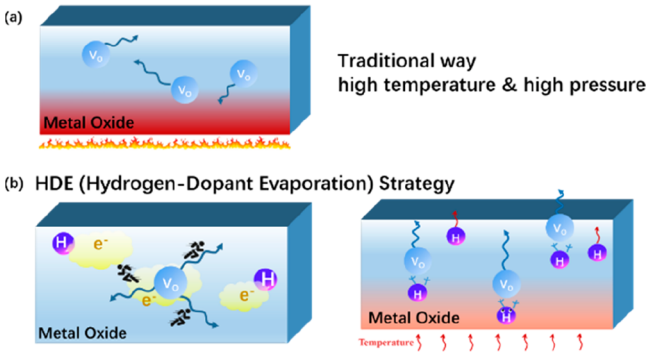


**Figure 1.** (a) Mechanism of the traditional thermal annealing process. (b) Schematic of the hydrogen-dopant evaporation strategy.

metal oxides at ambient conditions,[19] an alternative strategy of removing oxygen defects in metal oxides based on manipulation of hydrogen dopants is foreseeable.

In this work, we selected rutile $TiO_2$, rutile $SnO_2$, and monoclinic $VO_2$ as objects of investigation because they share the same coordination numbers and similar lattice topology. We built bulk models of $TiO_2$, $SnO_2$, and $VO_2$ with proper amounts of hydrogen dopants and performed both first-principles calculations and molecular dynamics (MD) simulation on these systems. We found that oxygen defects

**Received:** August 16, 2021
**Accepted:** September 24, 2021
**Published:** September 28, 2021

are prone to migrate with hydrogen doping, and nearby hydrogen atoms are mutually exclusive to oxygen defects because of the repulsive dipole interaction.[20]

Figure 1b depicts the mechanism of the hydrogen-dopant evaporation strategy. First of all, hydrogen doping increases the mobility of oxygen defects due to the accumulation of electrons in oxygen defects caused by hydrogen doping. Then, the generated dipole moments on both H and $V_O$ have repulsive interactions, which further incentivizes the diffusion of $V_O$. As the system is heated, the diffusion of H dopants will promote oxygen vacancies to flee to the surface, facilitating the repair of original bulk oxygen vacancies.

We chose rutile $TiO_2$, which crystallizes in a tetragonal cell with space group $P_{42}/mnm$, and built a $(2 \times 2 \times 2)$ supercell. The optimized structure supercell of rutile $TiO_2$ consists of 16 Ti atoms and 32 O atoms with the lattice parameters $a = b =$ 9.34 Å and $c = 6.06$ Å (Figure S1a), in good agreement with the reported experiment data.[21] Then, we created an oxygen vacancy in the supercell, which amounts to a defect concentration of ~3.13%. The optimized $TiO_2$–$V_O$ systems possess the lattice parameters $a = b = 9.37$ Å and $c = 6.09$ Å. Compared to the defect-free supercell of $TiO_2$, each dimension increased slightly by 0.03 Å upon introduction of one oxygen vacancy. Meanwhile, the Ti–O bond lengths for the Ti originally bonding with the removed O atom shortened by 0.03 Å to 0.17 Å because of pulling by the remaining O atoms bonding with these Ti atoms. In addition, the shape of cell changed from tetragonal to monoclinic ($\alpha = \beta = \gamma = 90° \rightarrow \alpha = \beta = 90°$, $\gamma = 90.49°$).

A hydrogen dopant can adopt either perpendicular or parallel orientation with respect to a Ti–O–Ti plane. A previous study[22] has shown that the energy for the perpendicular bonding state is lower than that for the parallel bonding state for r-$TiO_2$. The perpendicular bonding structure is used in our simulation. The optimized lattice constants of H-doped $TiO_2$ supercell are $a = 9.48$ Å, $b = 9.32$ Å, and $c = 6.12$ Å, showing a slight expansion of the lattice, similar to the system containing $V_O$. The structure distortion induced by an interstitial hydrogen mainly acts on the O atom that bonds with it and causes elongation of the three Ti–O bonds by 5–9% (Table S1).

Importantly, H-doping alters the electronic structure of the system. The differential charge density (Figure S2) shows charge transfer from the H atom to the neighboring O atoms. As a result, the H atom produces a dipole interaction with $V_O$. The DDEC6 method is used to compute the net atomic charges (NACs) and the atomic dipole moment. The dipole moment of a fragment is given by eq 1:[23]

$$\vec{\mu} = \sum_A q_A \vec{R}_A + \sum_A \vec{\mu}_A \tag{1}$$

where $q_A$ is the NAC of atom A, $\vec{R}_A$ is the atomic coordinate, and $\vec{\mu}_A$ is the atomic dipole moment. To estimate the interaction between the oxygen vacancy and the H dopant, we first defined the change of the dipole moments of the whole system due to introduction of the oxygen vacancy as the oxygen vacancy derived dipole. Within the point-dipole approximation, the coupling strength $J$ between $V_O$ and doping H can be expressed as eq 2:[24,25]

$$J = \frac{\vec{\mu}_{T,V_O} \cdot \vec{\mu}_H}{4\pi\varepsilon_0 r^3} - \frac{3(\vec{\mu}_{T,V_O} \cdot \vec{r})(\vec{\mu}_H \cdot \vec{r})}{4\pi\varepsilon_0 r^5} \tag{2}$$

where $\vec{\mu}_{T,V_O}$ is the oxygen vacancy transfer dipole, $\vec{\mu}_H$ is the doped H dipole, $\vec{r}$ is the position vector between the two fragments of the barycenter, and $\varepsilon_0$ is the vacuum permittivity. Figure 2a,b shows that the angle between the dipole moments

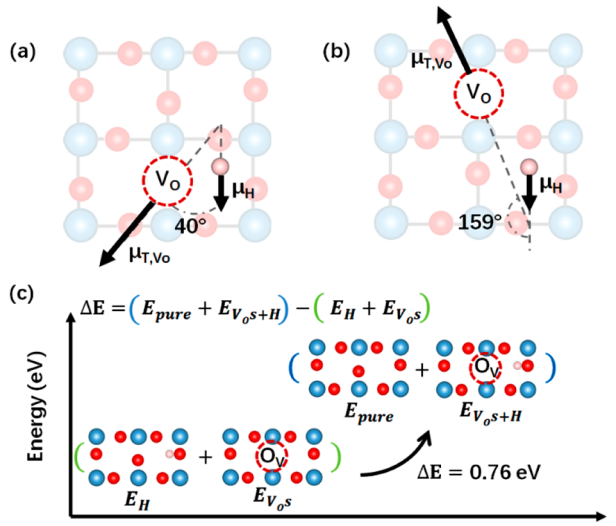


**Figure 2.** (a, b) The change of the dipole–dipole interaction between $V_O$ and doped H during $V_O$ migration. (c) Representation for repulsion of the oxygen defect and H in $TiO_2$.

changes from 40° to 159° as the $V_O$ moves away from H. Meanwhile, the energy change due to the dipole coupling is reduced by 0.1 eV, suggesting that the hydrogen and the oxygen defect tend to repel each other when they are close. We considered more oxygen defect structures with doped hydrogen in Figure S3 and Table S3, confirming the relationship between the dipole interaction and the distance. Figure 2c shows the energy required to drag an oxygen defect and H from infinity into the $TiO_2$ cell. We define the energy ($\Delta E$) induced by the interaction between $V_O$ and doped H in eq 3:

$$\Delta E = (E_{Vos+H} + E_{pure}) - (E_{Vos} + E_H) \tag{3}$$

where $E_{Vos+H}$, $E_{pure}$, $E_{Vos}$, and $E_H$ denote the energies of the structures of H-doped $TiO_2$ with $V_O$, pure $TiO_2$, $TiO_2$ with $V_O$, and H-doped $TiO_2$, respectively. For $TiO_2$, $\Delta E$ is 0.76 eV. The result suggests that $V_O$ and doped H have a repulsive interaction, which provides the potential for the oxygen vacancies to move.

To study the impact of H-doping on diffusion of $V_O$, we used the climbing-image NEB (CI-NEB) method to calculate the energy barrier of $V_O$ diffusion for different H-doping concentrations (the structures are shown in Figure S4). As shown in Figure 3a, the energy barriers for the $V_O$ migration go down from 1.03 to 0.52 eV as the concentration of H dopants increases from 0 to 4 per unit. Meanwhile, the ionic mobility of oxygen vacancy is calculated to be $2.83 \times 10^{-23}$, $1.40 \times 10^{-20}$, $1.57 \times 10^{-15}$, and $1.08 \times 10^{-14}$ $m^2$ $s^{-1}$ $V^{-1}$ in $TiO_{2-\delta}$, $H_{1/16}TiO_{2-\delta}$, $H_{1/8}TiO_{2-\delta}$, and $H_{1/4}TiO_{2-\delta}$, respectively. The ionic mobility is greatly improved with the increase of H-doping concentration. The promotion of migration of the oxygen vacancy by the H dopants is mainly due to the repulsive interaction between them.

In addition, the H dopant can steer the direction of the oxygen vacancy migration (Figure 3a,b). The whole system is


https://doi.org/10.1021/acs.jpclett.1c02687
J. Phys. Chem. Lett. 2021, 12, 9579–9583

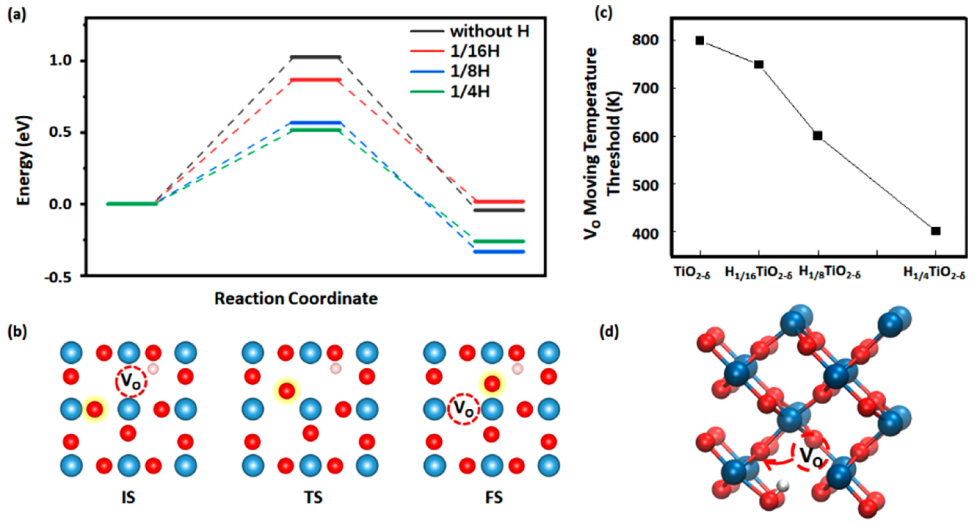


**Figure 3.** (a) Potential energy diagrams of $V_O$ migration for the different concentrations of H-doping. (b) Associated snapshots of the initial state (IS), the transition state (TS), and the final state (FS) in $H_{1/16}TiO_{2-\delta}$. (c) Minimum temperature needed for the oxygen vacancy migration as a function of the hydrogen dopant concentration. (d) Pathway of $V_O$ migration in $H_{1/16}TiO_{2-\delta}$ in molecular dynamics simulation.

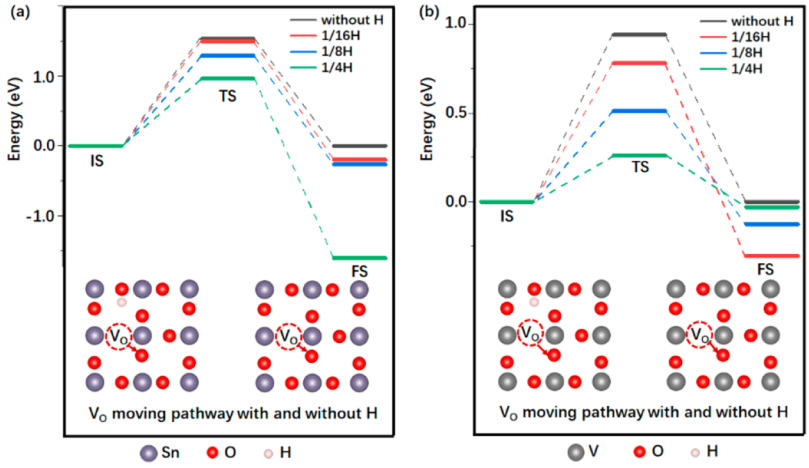


**Figure 4.** Impact of H-doping on the energy barrier of $V_O$ migration in (a) $SnO_2$ and (b) $VO_2$(M).

less stable when H and $V_O$ are adjacent (which is set as the initial state) and more stable as they are apart (which is set as the final state). Driven by thermodynamic energy, the oxygen vacancies tend to move away from the H dopant. Given that surface $V_O$ is more stable than bulk $V_O$ (Table S2), it is very likely that the H dopant will facilitate bulk $V_O$ to move out.

To verify the hydrogen-assisted $V_O$ diffusion mechanism, we performed molecular dynamics simulation with neural networks potential (NN-MD) at different temperatures as implemented in the LASP 2.3 package.[26,27] Consistent with the CI-NEB results, the energy needed for the $V_O$ diffusion, as reflected by the temperature threshold value, decreases with the increase of the H-doping concentration (Figure 3c). The lowering of the $V_O$ migration barrier also benefits from the hydrogen-doping-induced negative charges in the d orbitals of Ti atoms, which weaken Ti−O bonds and help $V_O$ movement.[28] This conjecture is supported by the simulation of migration of oxygen defect as an extra electron is added to the system which predicts a decrease of 0.14 eV for the energy barrier of $V_O$ migration (Figure S5). As expected, the temperature threshold for the $V_O$ migration is lowered from 800 to 750 K if hydrogen atoms are doped into the $TiO_{2-\delta}$ supercells (Figure 3d, Figure S6, and Movies S1−S8). If the H-doping concentration reaches $H_{1/4}TiO_{2-\delta}$, an achievable concentration,[19] $V_O$ will be able to migrate at 400 K, which not only is substantially below the temperature for the thermal annealing treatment[16] but also is comparable with the evaporation temperature of hydrogen dopants in metal oxides. Meanwhile, the potential competing between H diffusion and $V_O$ diffusion is investigated. As H atoms gain enough kinetic energies during the heating process, they can move toward oxygen vacancy as the latter is adjacent to the diffusion path of H atoms. The dynamic bonding between lattice O and diffusing H will also stabilize the H near the oxygen defect position. As one of the MD trajectories (Movie S9) shows, a hydrogen dopant moves to an oxygen vacancy as close as 4.4 Å and then oscillates. During the oscillation, H would push oxygen vacancy to move (Movie S10) due to their repulsive dipole−dipole interaction. Therefore, albeit the repulsion between H and $V_O$, H will be able to facilitate the migration of $V_O$.

We then used DFT calculations to examine the same hydrogen-dopant-assisted $V_O$ diffusion mechanism in $SnO_2$ and $VO_2$(M). The DFT computations revealed that these


https://doi.org/10.1021/acs.jpclett.1c02687
J. Phys. Chem. Lett. 2021, 12, 9579−9583

oxides have a similar topology to r-$TiO_2$. The migration pathways and the energy diagrams for the $V_O$ diffusion driven by the H-doping in the different concentrations are also determined (Figure 4). Just as in r-$TiO_2$, the energy barriers along the migration pathways in $SnO_2$ and $VO_2$(M) decrease with the H-doping, and the oxygen vacancy tends to migrate away from the H atom. The similarity in the impact of the H-doping on the $V_O$ migration suggests a general approach for treating bulk oxygen vacancies in metal oxides based on hydrogen doping. In addition, the energy barrier of oxygen defect migration in anatase-$TiO_2$ continuously decreases with the increase of H-doping concentration, which is in line with the simulation result of rutile $TiO_2$ (Figure S7).

In this work, we have considered $TiO_2$ as a representative system to demonstrate how hydrogen doping affects the mobility of oxygen vacancy and have found that hydrogen doping provides two driving forces for the oxygen vacancy migration. One is the charge accumulation at the oxygen vacancy that weakens the bond between the metal and oxygen atoms. The other is the repulsive dipole−dipole interaction between the hydrogen dopant and the oxygen vacancy that drives the migration of the oxygen defect associated with the hydrogen escape upon heating. On the basis of the mechanistic understanding, we have established a cost-effective approach to repair bulk oxygen vacancies in r-$TiO_2$ and similar metal oxides under mild conditions. Our work provides chemical and physical insights into the hydrogen-assisted oxygen defect repair and will guide the development of alternative ways of removal of bulk oxygen vacancies in metal oxides.

## ■ ASSOCIATED CONTENT

### Supporting Information

The Supporting Information is available free of charge at https://pubs.acs.org/doi/10.1021/acs.jpclett.1c02687.

Additional geometric and electronic structure data (PDF)
Movie S1 (AVI)
Movie S2 (AVI)
Movie S3 (AVI)
Movie S4 (AVI)
Movie S5 (AVI)
Movie S6 (AVI)
Movie S7 (AVI)
Movie S8 (AVI)
Movie S9 (AVI)
Movie S10 (AVI)

## ■ AUTHOR INFORMATION


### Corresponding Author

**Jun Jiang** − *Hefei National Laboratory for Physical Sciences at the Microscale, CAS Center for Excellence in Nanoscience, Collaborative Innovation Center of Chemistry for Energy Materials, School of Chemistry and Materials Science, University of Science and Technology of China, Hefei, Anhui 230026, P. R. China;* orcid.org/0000-0002-6116-5605; Email: jiangj1@ustc.edu.cn

### Authors

**Min Hu** − *Hefei National Laboratory for Physical Sciences at the Microscale, CAS Center for Excellence in Nanoscience, Collaborative Innovation Center of Chemistry for Energy Materials, School of Chemistry and Materials Science, University of Science and Technology of China, Hefei, Anhui 230026, P. R. China*

**Qing Zhu** − *Hefei National Laboratory for Physical Sciences at the Microscale, CAS Center for Excellence in Nanoscience, Collaborative Innovation Center of Chemistry for Energy Materials, School of Chemistry and Materials Science, University of Science and Technology of China, Hefei, Anhui 230026, P. R. China*

**Yuan Zhao** − *School of Physics and Optoelectronic Engineering, Ludong University, Yantai 264025, P. R. China*

**Guozhen Zhang** − *Hefei National Laboratory for Physical Sciences at the Microscale, CAS Center for Excellence in Nanoscience, Collaborative Innovation Center of Chemistry for Energy Materials, School of Chemistry and Materials Science, University of Science and Technology of China, Hefei, Anhui 230026, P. R. China;* orcid.org/0000-0003-0125-9666

**Chongwen Zou** − *National Synchrotron Radiation Laboratory, University of Science and Technology of China, Hefei 230029, P. R. China;* orcid.org/0000-0002-6153-081X

**Oleg Prezhdo** − *Department of Chemistry, University of Southern California, Los Angeles, California 90089, United States;* orcid.org/0000-0002-5140-7500

Complete contact information is available at: https://pubs.acs.org/10.1021/acs.jpclett.1c02687


### Author Contributions

M.H., Q.Z., and Y.Z. contributed equally to this work.

### Notes

The authors declare no competing financial interest.

## ■ ACKNOWLEDGMENTS

This work was financially supported by the National Key Research and Development Program of China (2018YFA0208603), the National Natural Science Foundation of China (22025304, 22033007), Anhui Initiative in Quantum Information Technologies (AHY090100), and the DNL Cooperation Fund CAS (No. DNL201913). O.V.P. acknowledges support of the US National Science Foundation (Grant CHE-1900510). The numerical calculations in this paper have been done in the Supercomputing Center of University of Science and Technology of China.

## ■ REFERENCES

(1) Ran, C.; Xu, J.; Gao, W.; Huang, C.; Dou, S. Defects in Metal Triiodide Perovskite Materials Towards High-Performance Solar Cells: Origin, Impact, Characterization, and Engineering. *Chem. Soc. Rev.* **2018**, *47* (12), 4581−4610.

(2) Fang, G.; Zhu, C.; Chen, M.; Zhou, J.; Tang, B.; Cao, X.; Zheng, X.; Pan, A.; Liang, S. Suppressing Manganese Dissolution in Potassium Manganate with Rich Oxygen Defects Engaged High-Energy-Density and Durable Aqueous Zinc-Ion Battery. *Adv. Funct. Mater.* **2019**, *29* (15), 1808375.

(3) Doherty, T. A. S.; Winchester, A. J.; Macpherson, S.; Johnstone, D. N.; Pareek, V.; Tennyson, E. M.; Kosar, S.; Kosasih, F. U.; Anaya, M.; Abdi-Jalebi, M.; Andaji-Garmaroudi, Z.; Wong, E. L.; Madeo, J.; Chiang, Y. H.; Park, J. S.; Jung, Y. K.; Petoukhoff, C. E.; Divitini, G.; Man, M. K. L.; Ducati, C.; Walsh, A.; Midgley, P. A.; Dani, K. M.; Stranks, S. D. Performance-Limiting Nanoscale Trap Clusters at Grain Junctions in Halide Perovskites. *Nature* **2020**, *580* (7803), 360−366.

(4) Youssef, M.; Van Vliet, K. J.; Yildiz, B. Polarizing Oxygen Vacancies in Insulating Metal Oxides under a High Electric Field. *Phys. Rev. Lett.* **2017**, *119* (12), 126002.

(5) Zhu, H.; Liu, Y.; Eickemeyer, F. T.; Pan, L.; Ren, D.; Ruiz-Preciado, M. A.; Carlsen, B.; Yang, B.; Dong, X.; Wang, Z.; Liu, H.; Wang, S.; Zakeeruddin, S. M.; Hagfeldt, A.; Dar, M. I.; Li, X.; Gratzel, M. Tailored Amphiphilic Molecular Mitigators for Stable Perovskite Solar Cells with 23.5% Efficiency. *Adv. Mater.* **2020**, *32* (12), No. e1907757.
(6) Hwang, T.; Lee, B.; Kim, J.; Lee, S.; Gil, B.; Yun, A. J.; Park, B. From Nanostructural Evolution to Dynamic Interplay of Constituents: Perspectives for Perovskite Solar Cells. *Adv. Mater.* **2018**, *30* (42), No. e1704208.
(7) Li, W.; She, Y. L.; Vasenko, A. S.; Prezhdo, O. V. Ab Initio Nonadiabatic Molecular Dynamics of Charge Carriers in Metal Halide Perovskites. *Nanoscale* **2021**, *13* (23), 10239−10265.
(8) Wan, J.; Chen, W.; Jia, C.; Zheng, L.; Dong, J.; Zheng, X.; Wang, Y.; Yan, W.; Chen, C.; Peng, Q.; Wang, D.; Li, Y. Defect Effects on $TiO_2$ Nanosheets: Stabilizing Single Atomic Site Au and Promoting Catalytic Properties. *Adv. Mater.* **2018**, *30* (11), 1705369.
(9) Zheng, D.; Peng, R.; Wang, G.; Logsdon, J. L.; Wang, B.; Hu, X.; Chen, Y.; Dravid, V. P.; Wasielewski, M. R.; Yu, J.; Huang, W.; Ge, Z.; Marks, T. J.; Facchetti, A. Simultaneous Bottom-up Interfacial and Bulk Defect Passivation in Highly Efficient Planar Perovskite Solar Cells Using Nonconjugated Small-Molecule Electrolytes. *Adv. Mater.* **2019**, *31* (40), 1903239.
(10) Zheng, J.; Lyu, Y.; Wang, R.; Xie, C.; Zhou, H.; Jiang, S. P.; Wang, S. Crystalline $TiO_2$ Protective Layer with Graded Oxygen Defects for Efficient and Stable Silicon-Based Photocathode. *Nat. Commun.* **2018**, *9* (1), 3572.
(11) Xiao, Z.; Huang, Y. C.; Dong, C. L.; Xie, C.; Liu, Z.; Du, S.; Chen, W.; Yan, D.; Tao, L.; Shu, Z.; Zhang, G.; Duan, H.; Wang, Y.; Zou, Y.; Chen, R.; Wang, S. Operando Identification of the Dynamic Behavior of Oxygen Vacancy-Rich $Co_3O_4$ for Oxygen Evolution Reaction. *J. Am. Chem. Soc.* **2020**, *142* (28), 12087−12095.
(12) Jeong, J.; Aetukuri, N.; Graf, T.; Schladt, T. D.; Samant, M. G.; Parkin, S. S. P. Suppression of Metal-Insulator Transition in $VO_2$ by Electric Field−Induced Oxygen Vacancy Formation. *Science* **2013**, *339* (6126), 1402−1405.
(13) Park, Y.; Sim, H.; Jo, M.; Kim, G. Y.; Yoon, D.; Han, H.; Kim, Y.; Song, K.; Lee, D.; Choi, S. Y.; Son, J. Directional Ionic Transport across the Oxide Interface Enables Low-Temperature Epitaxy of Rutile $TiO_2$. *Nat. Commun.* **2020**, *11* (1), 1401.
(14) Petrie, J. R.; Mitra, C.; Jeen, H.; Choi, W. S.; Meyer, T. L.; Reboredo, F. A.; Freeland, J. W.; Eres, G.; Lee, H. N. Strain Control of Oxygen Vacancies in Epitaxial Strontium Cobaltite Films. *Adv. Funct. Mater.* **2016**, *26* (10), 1564−1570.
(15) Zhao, X.; Xu, J.; Liu, L.; Lai, P.-T.; Tang, W.-M. Repair of Oxygen Vacancies and Improvement of $HfO_2/MoS_2$ Interface by $NH_3$-Plasma Treatment. *IEEE Trans. Electron Devices* **2019**, *66* (10), 4337−4342.
(16) Meyer, T. L.; Jacobs, R.; Lee, D.; Jiang, L.; Freeland, J. W.; Sohn, C.; Egami, T.; Morgan, D.; Lee, H. N. Strain Control of Oxygen Kinetics in the Ruddlesden-Popper Oxide $La_{1.85}Sr_{0.15}CuO_4$. *Nat. Commun.* **2018**, *9* (1), 92.
(17) Zhu, H.; Yang, Q.; Liu, D.; Du, Y.; Yan, S.; Gu, M.; Zou, Z. Direct Electrochemical Protonation of Metal Oxide Particles. *J. Am. Chem. Soc.* **2021**, *143* (24), 9236−9243.
(18) Li, B.; Hu, M.; Ren, H.; Hu, C.; Li, L.; Zhang, G.; Jiang, J.; Zou, C. Atomic Origin for Hydrogenation Promoted Bulk Oxygen Vacancies Removal in Vanadium Dioxide. *J. Phys. Chem. Lett.* **2020**, *11* (23), 10045−10051.
(19) Xie, L.; Zhu, Q.; Zhang, G.; Ye, K.; Zou, C.; Prezhdo, O. V.; Wang, Z.; Luo, Y.; Jiang, J. Tunable Hydrogen Doping of Metal Oxide Semiconductors with Acid-Metal Treatment at Ambient Conditions. *J. Am. Chem. Soc.* **2020**, *142* (9), 4136−4140.
(20) Fukagawa, H.; Hosoumi, S.; Yamane, H.; Kera, S.; Ueno, N. Dielectric Properties of Polar-Phthalocyanine Monolayer Systems with Repulsive Dipole Interaction. *Phys. Rev. B: Condens. Matter Mater. Phys.* **2011**, *83* (8), No. 085304.
(21) Burdett, J. K.; Hughbanks, T.; Miller, G. J.; Richardson, J. W.; Smith, J. V. Structural-Electronic Relationships in Inorganic Solids: Powder Neutron Diffraction Studies of the Rutile and Anatase Polymorphs of Titanium Dioxide at 15 and 295 K. *J. Am. Chem. Soc.* **1987**, *109* (12), 3639−3646.
(22) Pan, H.; Zhang, Y.-W.; Shenoy, V. B.; Gao, H. Effects of H-, N-, and (H, N)-Doping on the Photocatalytic Activity of $TiO_2$. *J. Phys. Chem. C* **2011**, *115* (24), 12224−12231.
(23) Hirshfeld, F. Bonded-Atom Fragments for Describing Molecular Charge Densities. *Theoret. Chim. Acta.* **1977**, *44* (2), 129−138.
(24) Zhang, Y.; Luo, Y.; Zhang, Y.; Yu, Y.-J.; Kuang, Y.-M.; Zhang, L.; Meng, Q.-S.; Luo, Y.; Yang, J.-L.; Dong, Z.-C.; Hou, J. G. Visualizing Coherent Intermolecular Dipole−Dipole Coupling in Real Space. *Nature* **2016**, *531* (7596), 623−627.
(25) Zhang, T.; Liu, Z. P.; Driver, S. M.; Pratt, S. J.; Jenkins, S. J.; King, D. A. Stabilizing Co on Au with $NO_2$: Electronegative Species as Promoters on Coinage Metals? *Phys. Rev. Lett.* **2005**, *95* (26), 266102.
(26) Huang, S.-D.; Shang, C.; Kang, P. L.; Zhang, X. J.; Liu, Z.-P. Lasp: Fast Global Potential Energy Surface Exploration. *Wiley Interdiscip. Rev.: Comput. Mol. Sci.* **2019**, *9* (6), No. e1415.
(27) Huang, S.-D.; Shang, C.; Zhang, X.-J.; Liu, Z.-P. Material Discovery by Combining Stochastic Surface Walking Global Optimization with a Neural Network. *Chem. Sci.* **2017**, *8* (9), 6327−6337.
(28) Wang, Z.; Wang, X.; Sharman, E.; Li, X.; Yang, L.; Zhang, G.; Jiang, J. Tuning Phase Transitions in Metal Oxides by Hydrogen Doping: A First-Principles Study. *J. Phys. Chem. Lett.* **2020**, *11* (3), 1075−1080.


https://doi.org/10.1021/acs.jpclett.1c02687
J. Phys. Chem. Lett. 2021, 12, 9579−9583